USM UNIVERSITI SAINS MALAYSIA

Program & Abstract Book

MAMIP 2012

Asian International Conference on Materials, Minerals, and Polymer

23rd - 24th March 2012, Vistana Hotel, Penang

Bridging Notions, Sustaining Innovations

Main Sponsors

RESEARCH AND INNOVATION

Springer

Organized by

Postgraduates Club PGSC School of Materials & Mineral Resources Engineering

MAMIP 2012

Surface Characteristic of Mesostructured Cellular Foam (MCF) Silica and Nickel Supported on the MCF Materials

Lilis Hermida[1,2], Ahmad Zuhairi Abdullah[1]*, Abdul Rahman Mohamed[1]
[1]School of Chemical Engineering, Universiti Sains Malaysia,
14300 Nibong Tebal, Penang, Malaysia.
[2]Department of Chemical Engineering, Universitas Lampung,
Bandar Lampung 35145, Lampung, Indonesia.
*Corresponding authors: chzuhairi@eng.usm.my

Abstract: *Surface characteristics of mesostructured cellular foam (MCF) silica materials prepared at an aging temperature of 80 ^{o}C and different aging times were investigated. The effect of nickel nanoparticle incorporation into these structures was also examined in terms of surface area, pore volumes and cell size and window pore size which were obtained from nitrogen adsorption-desorption measurements. The structures properties were also characterized using TEM and SEM analysis. The nitrogen adsorption-desorption measurements show that the window pore size increased with the aging time in the MCF silica synthesis. The window pore size of MCF silica material significantly affected the nickel nanoparticle incorporation.*

Keywords: MCF silica, Nickel catalyst, Pore structure, Surface characteristic

1. INTRODUCTION

Supported nickel catalysts have attracted research attention as heterogeneous catalysts because of their application in many important petrochemical industries such as hydrogenation, methanation, reforming, and hydrocracking. Besides nickel particle dispersion in catalyst support, it is found that pore size was a crucial variable affecting the catalyst performance, as the catalytic reactions rely on the presence of active centres located on the pore structures of the catalysts. Larger-pore sizes of catalyst provide better diffusion of reactants and products during the course of reactions. Therefore, well-dispersed the active centres on the high pore size are always desirable. Catalyst support may play a more active role in increasing the dispersion and stability of metal particles[1]. The main function of catalyst support is to keep up a fine dispersion of nickel particles and prevent the particle from aggregating relying on its confining nanosized environments [2].

Mesoporous silicas (such as MCM-4, SBA-15, HMS) having high surface area and high porosity (pore size of up to 10 nm) have been widely studied as a catalyst support for incorporation of sulphated metal oxides[3,4], platinum nanoparticles [5] and propyl sulfonic acid[6-8]. The mesoporous silicas have also been extensively used as supports for incorporation of nickel particles. Nickel functionalized mesoporous silicas hav been successfully applied for hydrochorination of chlorobenzene[9], catalytic reforming of methane with carbondioxide to produce synthesis gas (syngas)[10], hydrogenation of naphthalene[11], etc.

Mesostructured cellular foam (MCF) silica is a class of three-dimensional (3D) hydrothermally robust materials with ultra-large mesopores (up to 50 nm) [12-14]. In terms of the textural and framework structure, the MCF materials are composed of uniform spherical cells interconnected by window pores with a narrow size distribution [12]. Owing to their 3D mesopore system with pore sizes substantially larger than those of MCM-41 or SBA-15 mesostructures, MCF materials are known to have advantages in terms of better diffusion of reactants and products. This allows them to better overcome mass transfer limitations in many

reactions[14,15] . However, there has been quite limited information about the utilization of MCF silica as supports for loading of catalytically active component and there is no report in the literature dealing with dispersion of nickel particle on mesostructured cellular foam (MCF) silica so far.

In the present study, MCF silica materials with different mesostructure characteristics were prepared at various conditions in terms of aging time and used as support for nickel catalyst. Incorporation of nickel particle in the MCF silica was carried out using deposition and precipitation (DP) method followed by reduction process. Surface characteristics of the MCF silica materials prepared and their functionalization with nickel particle were examined by nitrogen adsorption-desorption measurements, TEM and SEM analysis.

2. EXPERIMENTAL

2.1. Preparation of MCF silica material

MCF silica materials with different structures were synthesized according to previously reported procedure [16] except the amount of acidic solution, the use of $NH_4F.HF$, the use of a lower aging temperature (80 ^oC) and various aging times. In a typical synthesis 4 g of P123 was dissolved in 70 ml of 1.6 M HCl. Then, 6.8 ml of TMB was added, and the resulting solution was heated to 40 ^oC with rapid stirring to synthesis of microemulsion (template). After stirring for 2 h, 9,2 ml of TEOS was added to the solution and stirred for 5 min. Then the solution was transfered into a poly-ethylene bottle at 40 ^oC in an oven for 20 h for formation of pre-condensed silica foam. After that, the mixture was removed from the oven and then $NH_4F.HF$ (92 mg in 10 ml DI water) was added to the mixture with slow mixing. Then the mixture was aged at 80 ^oC in the oven for certain aging time. Three samples were prepared for such mixtures, MCF-1D was aged for 1 day, MCF-2D was aged for 2 days and MCF-3D was aged for 3 days. After cooling, the mixture was filtered and then dried at 100 ^oC for 12 h. After that, calcination was carried out in static air at 300 ^oC for 0.5 h and 500 ^oC for 6 h to remove the template. The calcined MCF silica materials were used as support for Ni catalyst.

2.2. Incorporation of nickel catalyst on MCF silica materials

MCF-1D, MCF-2D and MCF-3D materials were then functionalized with nickel using deposition precipitation method adopted from Nares et al[11]. In the functionalization reaction. 250 ml of an aqueous solution containing 10.156 g of $Ni(NO_3)_2.6H_2O$ and 0.3 ml of HNO_3 69% wt/wt was prepared. In a typical preparation, 40 ml of the aqueous solution was used for dissolving 6.3 g urea at room temperature to produce a urea solution and 210 ml of the aqueous solution was mixed with 1.9 g of MCF silica materials to make a suspension. The suspension was heated at 40 ^oC, and then mixed with the urea solution under rapid mixing. After that, the mixture was heated to 90 ^oC for 2 h under static condition. After cooling, the mixture was filtered and the solid was washed three times with 20 ml distilled hot water (~50 ^oC), then dried at 100 ^oC for 12 h. Then, the solid was calcined in static air at 300 ^oC for 6 h. The calcined solids were designated as NiMCF-1D(C), NiMCF-2D(C) and NiMCF-3D(C). Then the samples were reduced at 550 ^oC for 2.5 h in hydrogen stream, and then cooled to room temperature under nitrogen flow. The reduced samples were designated as NiMCF-1D(R), NiMCF-2D(R) and NiMCF-3D(R).

2.3. Characterization

Nitrogen adsorption–desorption isotherms were measured using a Quanta-chrome Autosorb 1C automated gas sorption analyzer at liquid nitrogen temperature. Prior to the experiments, samples were degassed ($P < 10^{-1}$ Pa) at 270 ^oC for 6 h. The amount of nitrogen

gas adsorbed over a range of partial pressures at a single temperature was measured to obtain a graph known as an adsorption isotherm, whilst desorption isotherm was obtained by measuring the quantities of gas desorbed from the sample as the relative pressure was lowered. Specific surface areas were calculated using BET method (S_{BET}), while pore size distributions were obtained using the Barrett-Joyner-Halenda (BJH) model applied to adsorption and desorption isotherms data for cell and window pore sizes.

SEM images were capture using an Leo Supra 50 VP field emission SEM. TEM images were provided by Philips CM 12 transmission electron microscope. Before the TEM analysis, sample of about 0.08 g was first dissolved in a 5 ml of 100 % ethanol. Then, the solution was shaken for a moment; and subsequently a small amount of the solution was taken using a micropipette and dropped on a metal grid for the analysis.

3. RESULT AND DISCUSSION

Table 1 summarizes textural properties of various MCF silica supports prepared at different aging times and the corresponding nickel functionalized MFC catalysts after the reduction process. The textural properties were derived from nitrogen adsorption-desorption data using BJH method for cell and window pore size, and using BET method for total pore volume and surface area. For the MCF silica supports, window pore size generally increased with increasing aging time whilst cell size remained stable as can be seen from Table 1. The window pore sizes (from 125 A to 158 Å) were within mesoporous range. This result could be attributed to that the 'soft silica" –coated TMB/P123 microemulsion droplets (composite droplets) increased in size and expanding the window pore size in the composite droplets during the aging step at 80 ^{o}C. At the same time, condensation of silica in the walls continuously took place with the formation of Si-O-Si linkages solidifying inorganic network, and the materials with increased pore size gradually rigidified [17,18]. The longer duration of aging was attempted, the bigger increase of window pore size in MCF structure would be formed.

Table 1. Summary of the nitrogen-sorption results

Sample	S_{BET} (m^2/g)	V_{pore}(cm^3/g)	d_{cell} (Å)	$d_{window\ pore}$ (Å)
MCF-1D	394	1.85	235	125
MCF-2D	375	2.24	232	130
MCF-3D	378	2.12	235	158
NiMCF-1D(R)	253	0.93	233	153
NiMCF-2D(R)	281	1.02	184	125
NIMCF-3D(R)	307	1.09	234	90

d_{cell} and $d_{window\ pore}$ are the cell and window pore diameters, respectively, determined by the BJH method,[13] S_{BET} is the surface area determined by the BET method, and V_{pore} is the total pore volume determined at a relative pressure of 0.9948

The table also shows that total surface area decreased from 394 to 375 cm^2/g if the aging time was increased from 1 day to 2 days. The reduction of the BET surface areas with increased aging time might be related to the enlarged window pore sizes and denser framework walls [17,18]. However, the total surface area slightly increased from 375 to 378 cm^2/g if the aging time was increased from 2 days to 3 days. The increase in aging time from 1 day to 2 days resulted in an increase in total pore volume from 1.85 to 2.24 cm^3/g. Further increase in aging time to 3 days caused a slight decrease of the total pore volume to 2.12 cm^3/g. Moreover, incorporation of nickel particle on MCF silica materials resulted in a decrease in textural parameters like total surface area, total pore volume, cell size and window pore size.

The reduction of total pore volume of MCF materials after the functionalization can be confirmed by pore size distribution curves. The pore size distributions of cells and connecting window pores of MCF silica materials and nickel species functionalized MCF materials are shown in Figure 1. The figure shows strong evidences of pore volume reductions in which cell and window pore size distribution curves in nickel species functionalized MCF materials (NiMCF-1D(R), NiMCF-3D(R), and NiMCF-3D(R)) were smaller compared to those in MCF materials. Furthermore, functionalization of MCF-1D resulted in a bimodal window pore size distribution with maximum peaks at around 30 Å and 150 Å. The maximum peak in window pore size distribution of MCF-1D parent material was at around 150 Å. Meanwhile, the maximum peak of cell size distribution (at about 230 Å) in MCF-1D did not change after the functionalization. Functionalization of MCF-2D resulted in a decrease in the maximum peak of cell size distribution from about 230 to 200 Å but the maximum peak of window pore size distribution (at about 130 Å) in MCF-2D was about the same as that in the nickel functionalized MCF-2D material. Different observation was made for MCF-3D material, in which maximum peak in window pore size distribution was much lower after the functionalization with nickel species. The observed reduction of pore volume, cell and window pore sizes of nickel species functionalized MCF materials were attributed to the attachment of the desired nickel species to the pore surface.

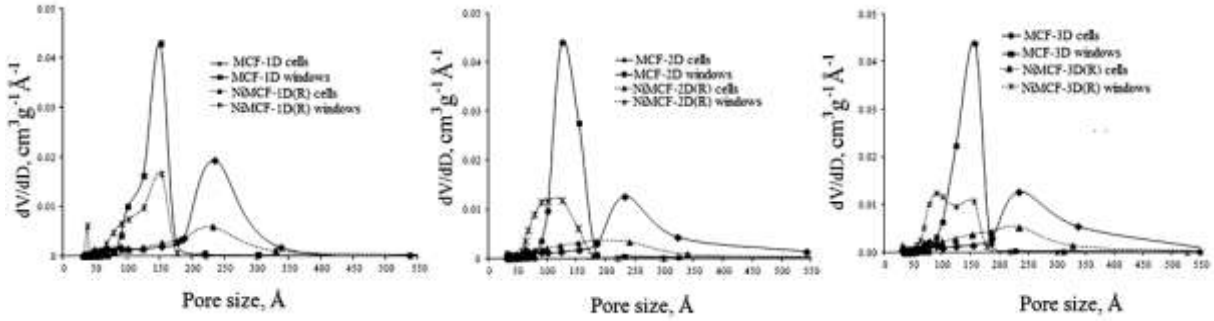

Figure 1. Cell and window pore size distribution of MCF silica materials and nickel species functionalized MCF silica after reduction process

Nitrogen adsorption-desorption isotherms for MCF silica materials shown in Figure 2 are of type IV as hysteresis occurs in multilayer range of physisorption isotherms. This hysteresis is often associated with capillary condensation (the pore filling process) in mesopore structure [19]. The nitrogen adsorption-desorption isotherms are in close agreement with those published previously [12,13,17,18] and exhibit a large H1 hysteresis loop, which suggests that the MCF material possesses cell-type mesopores connected by smaller window pores. According to IUPAC (International Union of Pure and Applied Chemistry) recommendation, pores with diameter not exceeding 20 Å are defines as micropores, while mesopores are pores with diameter between 20 and 500 Å, and macropores represent pores with diameter greater than 500 Å [19]. Type IV adsorption isotherms usually flatten at high P/P0 indicating that the mesopore filling was complete [20]. However, final upward turn was observed for all the isotherm curves as shown in Figure 2. This was due to capillary condensation in macropores or in interstices between grains as reported in the literature [21].

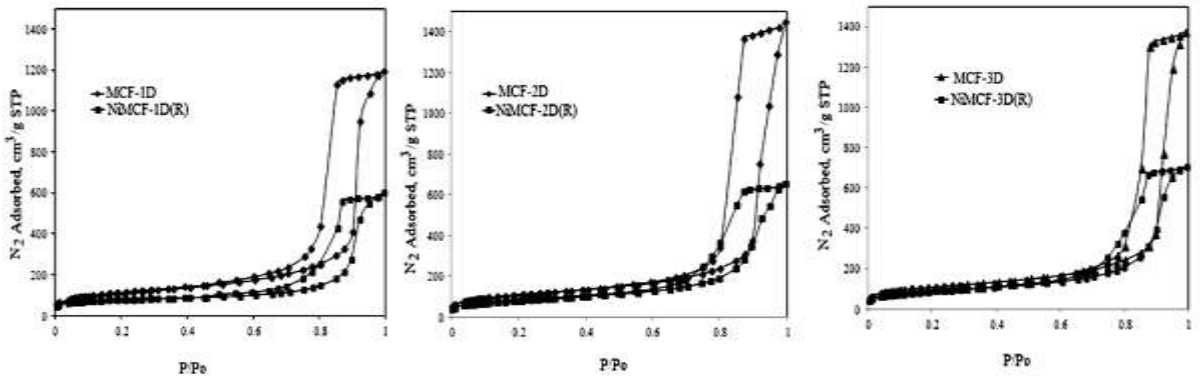

Figure 2. Nitrogen adsorption-desorption isotherm of MCF silica materialand nickel species functionalized MCF silica after reduction process.

Surface functionalization of MCF silica materials with nickel species followed by reduction process in hydrogen flow at 550 ^{o}C, i.e. NiMCF-1D(R), NiMCF-2D(R), NiMCF-3D(R), resulted in lower isotherm curves but no appreciable change in the form of the isotherms (Figure 2). This indicates that total pore volume decreased but the mesoporosity of the MCF materials was maintained after functionalization. Furthermore, it can be noted that, for MCF-3D material, the functionalization resulted in the highest isotherms compared to MCF-1D and MCF-2D materials, possibly indicating the lowest densification of the silica walls.

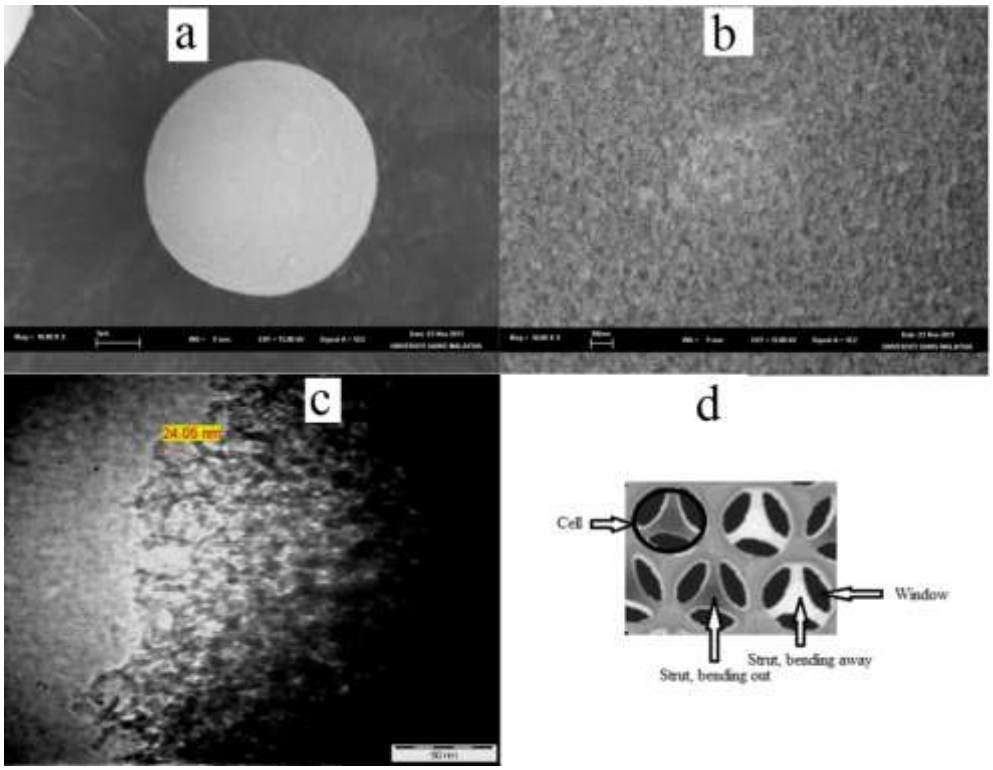

Figure 3, (a) SEM image of MFC-3D morphology, the scale bar represents 1μm. (b) A higher magnification image showing the morphology of the MCF-3D surface. (c) TEM image of MCF-3D, the scale bar represents 50 nm. (d) Schematic cross section of MCF material[18].

Figure 3(a) shows scanning electron microscope (SEM) image of MCF-3D material that clearly confirmes a spherical particle of MCF-3D with a size of about 5 μm in diameter. A higher magnification SEM image (Figure 3(b)), and transmission electron microscopy (TEM) image (Figure 3(c)) show that MCF-3D possessed a mesoporous structure with cell size of about 240.5 Å (24.05 nm), which was consistent with the average cell size (235 Å) obtained from nitrogen adsorption-desorption data (Table 1). The TEM image also confirmed a disordered array of silica struts composed of uniform-sized spherical cells interconnected by window pores with a narrow size distribution, which is the characteristic structural feature of MCF material [12,18]. It has been reported in the literature that schematic cross section of MCF material is of strutlike structure, as given in Figure 3 (d), showing that the cells of the MCF structure are framed by the silica struts [18].The wall thickness of the MCFs estimated by TEM is about 5 nm, in agreement with the thick, robust framework walls observed in MCF-type mesoporous silica as reported in the literature [18].

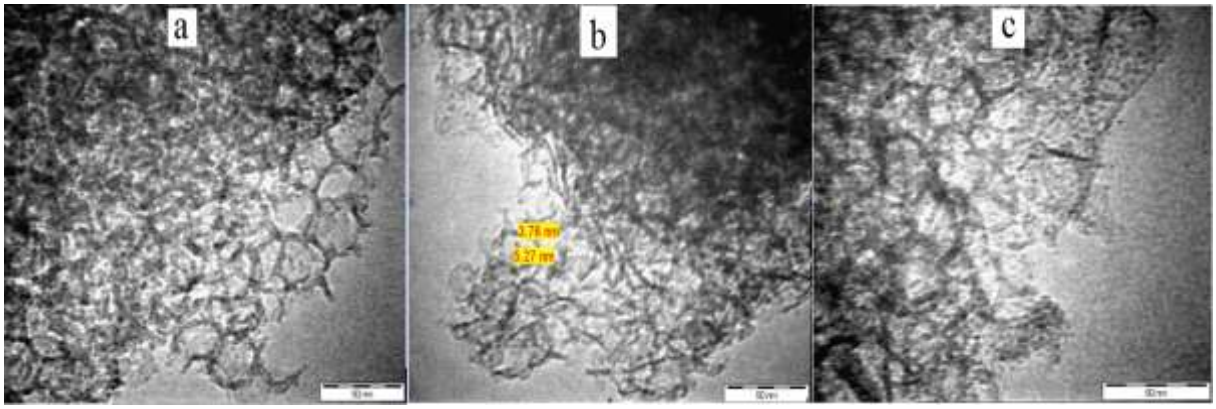

Figure 4. TEM images of (a) NiMCF-1D(R), (b) NiMCF-2D(R) and (c) NiMCF-1D(R)

Functionalization of MCF silica materials with Ni that were prepared at different aging times (MCF-1D, MCF-2D and MCF-3D) with nickel species followed by reduction process resulted in dispersed nickel particles on the MCF silica materials, as shown though TEM images in Figure 4. The figure clearly shows that nickel nanoparticles visible as dark spots were successfully distributed inside the pore of MCF materials and their mesostructures were preserved after the functionalization. This result was consistent with that reported by Na-Chiangmai et al.[22] who observed that functionalization of MCF material with Pd nanoparticles had no significant influent on structure of the mesoporous host material. For NiMCF-1D(R) and NiMCF-2D(R) prepared using MCF host with aging time for 1 and 2 days, respectively, spherical Nickel particles with sizes about 3.76 – 5.27 nm and irregular shape were found to be dispersed on the MCF supports as shown in Figure 4 (a) and 4 (b). However, for NiMCF-3D(R) prepared using MCF host with aging time for 3 days, a narrow nickel particle size distribution and much smaller nickel particles with a mean particle size about 1-2 nm were observed. Through the TEM images it can be noted that the amount of nickel nanoparticles particles observed in NiMCF-3D(R) was the highest compared to that in NiMCF-1D(R) and NiMCF-2D(R). The amount of nickel nanoparticles dispersed on the MCF materials seems to decrease in the order NiMCF-3D(R) > NiMCF-2D(R)> NiMCF-1D(R).

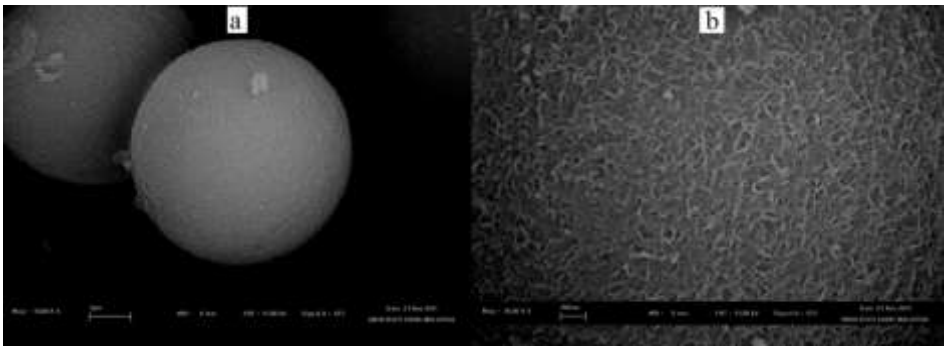

Figure 5. SEM image of NiMFC-3D(R) morphology, the scale bar represents 1μm. (b) A higher magnification image showing the morphology of the NiMFC-3D(R) surface,

It could be envisioned that window pore size of MCF material used as a host was the main factor that influenced the nickel nanoparticle incorporation. The window pore size of MCF host prepared using aging time of 3 days (MCF-3D) was the highest among the others and window pore size of MCF-2D was higher than that of MCF-1D, as presented in Table 1. As such, most of nickel nanoparticle could be easily introduced through the window pore size of MCF-3D host. This results in the highest amount of nickel nanoparticles in the NiMCF-3D(R). It can be concluded that larger window pore size of MCF host resulted in the easier incorporation of nickel nanoparticle with smaller sizes. Figure 5 (a) showing SEM image of NIMCF-3D(R) particles clearly confirms their spherical shape of about 5 μm in diameter which was maintained after nickel nanoparticle incorporation. A higher magnification SEM image in Figure 5 (b) shows that the uniform nickel nanoparticles in the form of nanoworms were well dispersed in the framework of the MCF-3D host. Hence, a suitable host was necessary for obtaining a high dispersion of nickel species with small size into the mesoporous framework

4. CONCLUSIONS

Incorporation of nickel nanoparticles into MCF silica materials prepared at aging temperature of 80 ^{o}C and various aging times (1, 2 and 3 days) was successfully carried out. The increase in aging time resulted in increase in window pores size in the MCF materials. Meanwhile, total surface area and pore volume tended to decrease. The nickel nanoparticle incorporation into the MCF silica materials was prepared using deposition-precipitation method at 90 ^{o}C for two hours followed by reduction process for 2.5 h at 550 ^{o}C. The window size was deemed the critical dimension controlling for the nickel nanoparticle incorporation. Among the MCF silica with various window pore sizes used in this study, MCF-3D with the highest window pore size was the best host for the nickel nanoparticle incorporation as most of nickel particles with small sizes were easily introduced as confirmed in TEM analysis results.

5. REFERENCES

1. Taylor, W. F., Yates, D. J. C., and Sinfelt, J. H. (1964). Catalysis over supported metals II. The effect of the support on the catalytic activity ofnickel for ethane hydrogenolysis. *J. Phys. Chem.*, 68, 2962- 2966.
2. Niu, K., Shi, D., Dong, W., Chen, M., Zhongbin. N. (2011). Chelating template-induced encapsulation of NiO cluster in mesoporous silica via anionic surfactant-templated route. *J. Colloid Interface Sci.*, 362, 74–80.

3. Hermida, L., Abdullah, A.Z., Mohamed, A.R. (2010). Post synthetically functionalized SBA-15 with organosulfonic acid and sulphated zirconia for esterification of glycerol to monoglyceride. *J. App. Sci*., 10 (24), 3199–3206.
4. Degirmenci, V., Yilmaz, A., Uner, D. (2009). Selective methane bromination over sulfated zirconia in SBA-15 catalysts. *Catal. Today.* 142, 30–33.
5. Huang, T., Tu, W. (2009). Modification of functionalized mesoporous silica on the formation and the catalytic performance of platinum nanocatalysts. *Appl. Surf. Sci.*, 255, 7672–7678.
6. Hermida, L., Abdullah, A.Z., Mohamed, A.R. (2011). Synthesis of monoglyceride through glycerol esterification with lauric acid over propyl sulfonic acid post-synthesis functionalized SBA-15 mesoporous catalyst. *Chem. Eng. J.*, 174, 668– 676.
7. Kureshy, R.I., Ahmad, I., Pathak, K., Khan, N.H., Abdi , S.H.R., Jasra, R.V.(2009). Sulfonic acid functionalized mesoporous SBA-15 as an efficient and recyclable catalyst for the synthesis of chromenes from chromanols. *Catal. Commun.*, 10, 572–575.
8. Hermida, L., Abdullah, A.Z., Mohamed, A.R. Effects of functionalization conditions of sulfonic acid grafted SBA-15 on catalytic activity in the esterification of glycerol to monoglyceride: a factorial design approach. *J. Porous Mater.* in press.
9. Chen, J., Zhou, J., Wang, R., Zhang, J. (2009). Preparation, characterization, and performance of HMS-supported Ni catalysts for hydrodechlorination of chorobenzene. *Ind. Eng. Chem. Res., 48,* 3802–3811.
10. Liu, D., Lau, R., Borgna, A., Yang Y. (2009). Carbon dioxide reforming of methane to synthesis gas over Ni-MCM-41 catalysts. *Appl. Catal. A.*, 358, 110–118.
11. Nares, R., Ramırez, J., Gutierrez-Alejandre, A., Cuevas, R. (2009).Characterization and hydrogenation activity of Ni/Si(Al)- MCM-41 catalysts prepared by deposition-precipitation. *Ind. Eng. Chem. Res. 48,* 1154–1162.
12. Schmidt-Winkel, P., Lukens Jr., W.W., Zhao, D., Yang, P., Chmelka, B.F., Stucky, G.D. (1999). Mesocellular siliceous foams with uniformly sized cells and windows. *J. Am. Chem. Soc.,* 121 254-255.
13. J.S. Lettow, Y.J. Han, P. Schmidt-Winkel, P. Yang, D. Zhao, G.D. Stucky, J.Y. Ying, Hexagonal to mesocellular foam phase transition in polymer-templated mesoporous silicas. *Langmuir*, 16 (2000) 8291-8295.
14. On, D.T., Kaliaguine, S. (2003). Zeolite-coated mesostructured cellular silica foams. *J. Am. Chem. Soc*.,125, 618-619.
15. Han, Y.J., Watson, J.T., Stucky, G.D., Butler, A. (2002). Catalytic activity of mesoporous silicate-immobilized chloroperoxidase . *J. Mol. Catal, B.*, 17, 1-8.
16. Han, Y., Lee, S. S., Ying, J. Y. (2010). Siliceous mesocellular foam for high-performance liquid chromatography: Effect of morphology and pore structure. *J. Chromatogr. A.* 1217, 4337–4343
17. Schmidt-Winkel, P, Glinka, C.J, Stucky, G.D. (2000).Microemulsion templates for mesoporous silica. *Langmuir,* 16, 356- 361.
18. Schmidt-Winkel, P, Lukens,W.W, Yang, P., Margolese, D.L., Lettow, J.S., Ying, J.Y., Stucky, G.D. (2000). Microemulsion templating of siliceous mesostructured cellular foams with well-defined ultralarge mesopores. *Chem Mater*., 12, 686-696.
19. Sing, K.S.W. (1998). Adsorption methods for the characterization of porous materials. *Adv. Colloid Interface Sci.,* 76 – 77, 3-11.
20. Barton, T. J., Bull, L. M., Klemperer, W. G., Loy, D. A., McEnaney, B., Misono, M., Monson, P. A., Pez, G., Scherer, G. W., Vartuli, J. C., and Yaghi, O. M. (1999). Tailored porous materials. *Chem. Mater.,* 11, 2633-2656.

21. Sing, K.S.W., Everett, D.H., Haul, R.A.W., Moscou, L., Pierotti, R.A., Rouquerol J., Siemieniewska, T. (1985). Reporting physisorption data for gas/solid systems with special reference to the determination of surface area and porosity. *Pure Appl. Chem.*, 57, 603–619.
22. Na-Chiangmai, C., Tiengchad, N., Kittisakmontree, P., Mekasuwandumrong, O., Powell, J., Panpranot, J. (2011). Characteristics and catalytic properties of mesocellular foam silica supported Pd nanoparticles in the liquid-phase selective hydrogenation of phenylacetylene. *Catal. Lett.*, 141, 1149–1155.